An electrically driven terahertz metamaterial diffractive modulator with more than 20 dB of dynamic range

N. Karl,[1] K. Reichel,[1] H.-T. Chen,[2] A. J. Taylor,[2] I. Brener,[3] A. Benz,[3] J. L. Reno,[3] R. Mendis,[1] and D. M. Mittleman[1]
[1]*Department of Electrical and Computer Engineering, Rice University, MS 378, Houston, Texas 77251-1892, USA*
[2]*Center for Integrated Nanotechnologies, Los Alamos National Laboratory, P. O. Box 1663, MS K771, Los Alamos, New Mexico 87545, USA*
[3]*Center for Integrated Nanotechnologies, Sandia National Laboratories, P. O. Box 5800, MS 1082, Albuquerque, New Mexico 87185, USA*

(Received 13 January 2014; accepted 19 February 2014; published online 4 March 2014)

We design and experimentally demonstrate a switchable diffraction grating for terahertz modulation based on planar active metamaterials, where a Schottky gate structure is implemented to tune the metamaterial resonances in real-time via the application of an external voltage bias. The diffraction grating is formed by grouping the active split-ring resonators into an array of independent columns with alternate columns biased. We observe off-axis diffraction over a wide frequency band in contrast to the narrow-band resonances, which permits operation of the device as a relatively high-speed, wide-bandwidth, high-contrast modulator, with more than 20 dB of dynamic range. © *2014 AIP Publishing LLC*. [http://dx.doi.org/10.1063/1.4867276]

The terahertz (THz) region of the electromagnetic spectrum has been identified as a significant area of research for a number of years, yet progress has been slow due to the challenges involved with THz generation, detection and manipulation.[1] The development of effective THz modulators, particularly using an electrical approach, is an active research field as it will enable a wide range of applications including signal processing and beam steering. Early demonstrations of electrically controlled THz modulators were based on semiconducting two-dimensional electron-gas (2DEG) structures[2,3] or birefringent liquid crystals.[4] However, each of these existing designs suffers from various drawbacks that limit their use, e.g., the requirement of cryogenic temperature for operation,[2] a limited modulation depth,[3] or a slow modulation speed.[4] Taking advantage of the controllable intraband transitions of graphene, Sensale-Rodriguez *et al.* highlighted the interesting applications graphene may have in the THz range by demonstrating a graphene-based electrical THz modulator with very low intrinsic signal attenuation, having the drawback of limited modulation depth.[5] The resolution of such weaknesses continues, as we have recently reported a technique for increased modulation depth in graphene-based modulators via the use of ring-shaped apertures near the graphene layer.[6] Furthermore, emergent opportunities have come from the development of metamaterials in which distinct materials can be integrated, forming hybrid metamaterial based THz modulators with improved performance. Such modulators have been actively pursued with the expectation of overcoming these drawbacks.[7–11]

Metamaterials are artificial materials that can be engineered to exhibit properties that are not found in ordinary materials.[12,13] Of particular interest for THz modulation are planar metamaterials that can be electrically switched.[14] This switching provides a mechanism for high-speed modulation of THz radiation, a result that is otherwise difficult to achieve. However, these planar metafilms exhibit a relatively low on/off ratio (<10 dB[9]), which may limit their applicability. Various related designs have been proposed to address this issue, including switchable plasmonic devices based on extraordinary optical transmission,[15,16] micro-electro-mechanical-systems (MEMS) based metamaterial devices,[17] or devices based on metal-insulator transition materials such as VO_2 that exhibit strongly temperature-dependent properties.[18,19] As an alternative, one can take advantage of the fact that an array of metamaterial split-ring resonator (SRR) elements can be grouped into "pixels,"[20] and that these groups can be engineered into patterns composing the overall structure of the array. This permits us to design an electrically controlled diffractive modulator in the spirit of a conventional acousto-optic modulator.[21] In this Letter, we report the demonstration of a first-generation device showing an electrically controllable diffraction pattern.

The metamaterial device consists of a planar array of sub-wavelength sized electric split-ring resonators (eSRRs)[22] fabricated on a 1-μm-thick *n*-doped GaAs epilayer grown on an intrinsic GaAs substrate.[7–9] The eSRR elements, as shown in Fig. 1(a), are interconnected with metallic wires and grouped into independent, periodic, columns each with a contact pad for external electrical control, shown in Fig. 1(b). As in previous switchable metamaterial devices,[7–9,20] the *n*-doped substrate epilayer effectively increases the damping (i.e., shorting out the split gaps) in the eSRRs, thus eliminating the *LC* resonance of the metamaterial.[7] However, the application of a DC bias to the metallic structure creates a depletion region in the narrow gaps, which restores the capacitive split gaps and thus also the THz resonance.[7]

The eSRR layout (into groups) is similar in concept to our previously described THz spatial light modulator (SLM) which had a different pixelization scheme that also used independently switchable groups of eSRRs.[20] In our earlier device, the pixels had a square geometry, and consisted of 2500 subelements; the device had a collection of 16 pixels forming a

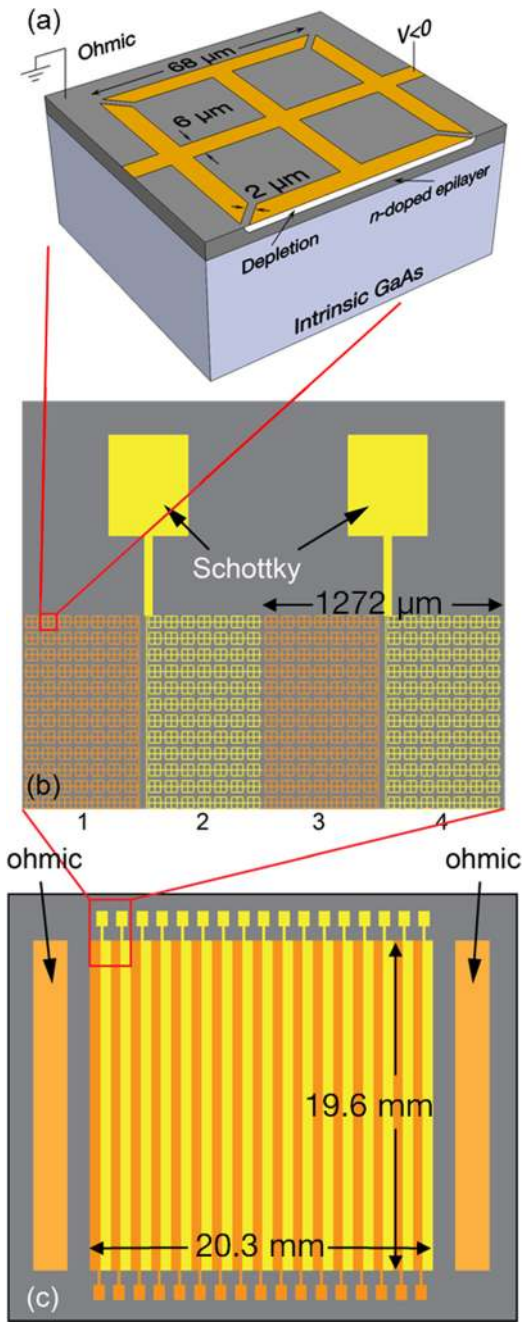

FIG. 1. (a) Unit cell of the metamaterial, illustrating a single eSRR element in the reverse biased state. The dark gray region shows the higher carrier density in the *n*-doped GaAs epilayer, and the white region around the cut-away portion of the metal structure indicates the depletion upon a reverse voltage bias. (b) Schematic showing a portion of the first four "pixels," which are composed of the eSRRs in (a) The eSRRs are patterned in rows, seven across, and interconnected, forming a Schottky gate; the pads of the first two even columns are displayed. (c) Illustration of the entire metamaterial grating (consisting of 32 columns). The color profile illustrates that alternate columns are biased forming a diffraction grating, with each column being independently controlled by the voltage bias between its Schottky pad and the Ohmic contacts.

4×4 grid, which made up the metamaterial array.[20] In the present device, the "pixels" are rectangular in shape, forming columns. Each column has a width of 596 μm and consists of rows of seven eSRRs. The eSRRs have an outer dimension of 68 μm, a metal strip width of 6 μm and thickness of 200 nm, a split gap of 2 μm, and a periodicity of 88 μm. In all, the device has 32 columns, as shown in Fig. 1(c), with two columns forming the periodic unit. The two columns are separated by 60 μm allowing for connecting wires to their individual contact pads (the odd columns' pads are along the bottom of the device and the even columns' pads are along the top) so that they can be addressed by an external voltage, and the metamaterial resonance can be switched on and off. The spacing between consecutive two-column units is 20 μm, the same as the spacing between eSRRs. This gives a two-column periodicity of $d = 1272\ \mu$m. The final metamaterial device has an active area of $19.6 \times 20.3\ \text{mm}^2$.

For this device, the size and structure of the eSRR elements are chosen such that a metamaterial resonance occurs at 0.4 THz (corresponding to a free-space wavelength $\lambda_0 = 0.75$ mm). This wavelength λ_0 is comparable to the column width of the device. When we apply a DC bias to alternate columns, the transmission at the resonance frequency is modulated periodically across the face of the device. In this configuration the device operates as a grating, and so we would expect to observe radiation diffracted at an angle to the normally incident direction. The first-order diffraction angle is given by $\sin(\theta) = \lambda/d$, which corresponds to $\theta = 36.1^\circ$ at λ_0. If we remove the DC bias from all of the columns (or apply it equally to all columns), then the diffracted beam should disappear since there is no longer a periodic variation of the transmission function. Thus, as we apply and remove a voltage from alternate columns of the metamaterial, we expect that the diffracted signal will be modulated with a very large dynamic range (i.e., in the diffraction direction the signal should be effectively background-free).

To observe the expected diffraction, we characterize our device using a THz time-domain spectroscopy system in transmission geometry with fiber-coupled photoconductive antennae for both THz generation and detection (see Fig. 2). The linearly polarized THz beam is collimated and directed towards the metamaterial at normal incidence, with the polarization of the THz electric field oriented parallel to the long axis of the metamaterial columns, i.e., in the vertical direction and perpendicular to the interconnecting metal wires.[7] The THz beam spot on the device has a diameter (1/e) of approximately 6 mm, large enough to illuminate numerous columns but small enough to avoid scattering from the metal mounting hardware at the edges of the device. The back surface of the GaAs substrate is uncoated, making further device optimization using an anti-reflection coating

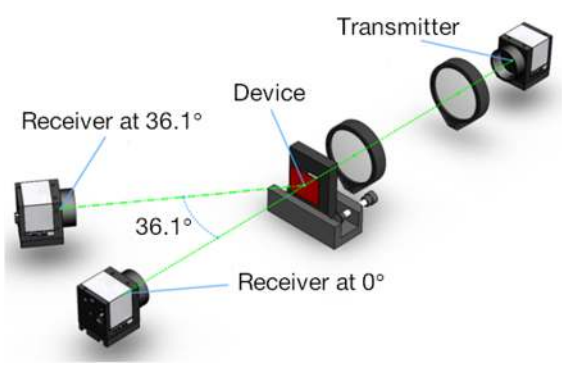

FIG. 2. Schematic of the experimental configuration used for THz transmission measurements of the device. The receiver is mounted on a stage allowing angular positioning; the on-axis and $\theta = 36.1^\circ$ receiver locations are shown.

possible. The receiver is positioned at a distance of 25 cm from the device at various angular positions relative to the axis of the incident beam.

We measure the THz signal using two methods. In the first method, we apply a DC voltage bias to alternate (or all) metamaterial columns, and insert an optical chopper into the THz beam before it interacts with the device, using a lock-in amplifier referenced to the chopper frequency. Using this method, we are able to directly measure the diffracted beam as well as the zero-order beam. Therefore, this configuration permits us to determine the strength of the on-axis metamaterial modulation, the diffraction efficiency, and the insertion loss. Fig. 3 shows the spectra of the transmitted zero-order radiation under normal incidence using this measurement method. When a reverse voltage bias (−13 volts) is applied to all columns of the metamaterial array we clearly observe the spectral dip at the designed metamaterial resonance frequency of 400 GHz (shown in red). This is in contrast to the absence of a spectral feature when the columns are all grounded (shown in black).

In the second method, we apply a square-wave AC voltage oscillating between 0 and −13 volts at 1 kHz to alternate (or all) metamaterial columns. This frequency is also used as the reference to a lock-in amplifier. Thus we are essentially performing a differential measurement that provides the signal difference between the diffracted signals with and without electrical bias. In experiments with normal incidence, we sweep the receiver angle, and keep the distance to the device fixed. Fig. 4(a) shows the measured signal (using the second method) as a function of receiver angular position. Here, we obtain THz waveforms at each receiver angular position, and then extract the magnitude of the spectral component at 0.4 THz by Fourier transform. We display the results for two different biasing conditions. The red curve shows the differential signal when the AC bias is applied to alternate columns, thus representing the relative strength of the diffracted signal. In contrast, the black curve shows the differential signal when the same AC bias is applied to all of the columns such that no diffraction should occur, representing the background signal. Nominally, the background should be zero in the diffraction direction; however, some small background signal is observed, due to two possible factors. First, small random scattering may occur due to roughness or imperfections in the eSRR pattern. Second, the normally incident Gaussian beam may be slightly diffracted naturally after passing through the device, resulting in a small signal even at large angles to the normal direction. The effect of diffraction is likely more dominant, however we are unable to experimentally rule out the effect of scattering from roughness. Nevertheless, when the bias is applied to alternate columns we observe a clear signature of diffraction at 0.4 THz at an angle of $\theta = \sim 36°$, consistent with the anticipated diffraction angle for this grating geometry.

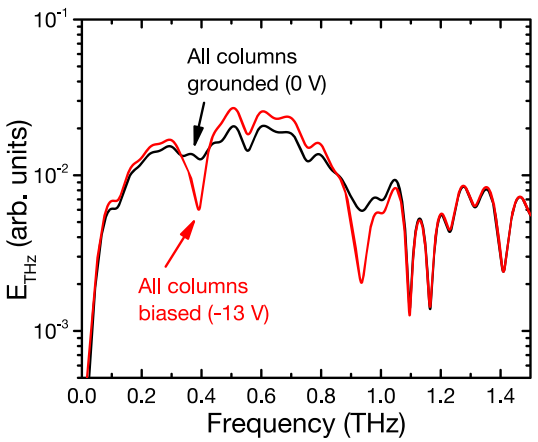

FIG. 3. The THz electric field amplitude modulation of the metamaterial at normal incidence, showing the effect of applied gate bias on the metamaterial resonance at 400 GHz.

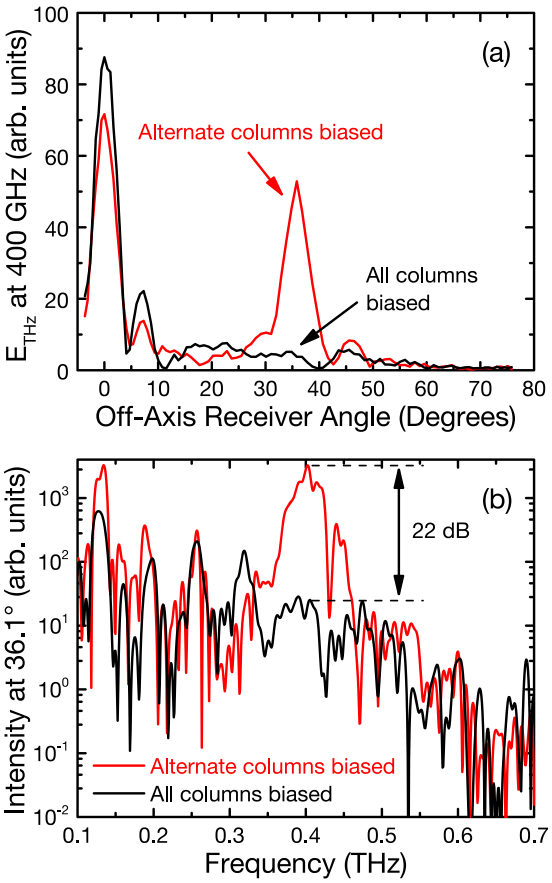

FIG. 4. (a) The angular dependence of the differential diffracted THz electric field amplitude at 400 GHz, when applying an alternating bias at 1 kHz to the device. A strong diffracted signal at ∼36° is observed when alternate columns are biased (red), creating a diffraction grating. In contrast, when all columns are biased (black) the grating effect disappears. (b) The intensity spectra of the differential signals diffracted at 36.1°, when applying an alternating bias at 1 kHz to the device. A 22 dB modulation depth is achieved at 400 GHz. The red curve shows the intensity when alternate columns are biased (acting as a grating). In contrast, the black curve represents the background, showing the intensity when all of the columns are biased.

To determine the modulation capability of our device, we investigate the entire available spectrum (not just the 400 GHz component) at the angle of the diffraction peak. Fig. 4(b) shows the spectral response at the peak of the first-order diffracted signal (i.e., at $\theta = 36.1°$), plotted on a log scale. We observe a modulation depth of ∼22 dB at the design frequency of 400 GHz. This represents the largest dynamic range of an electrically controlled THz modulator yet reported.

It has been shown that these electrically switchable eSRR arrays exhibit correlated amplitude and phase modulation over a relatively broad bandwidth, not merely at the frequency of the eSRR resonance.[9] Thus we anticipate that other frequency components of the broadband THz illumination will

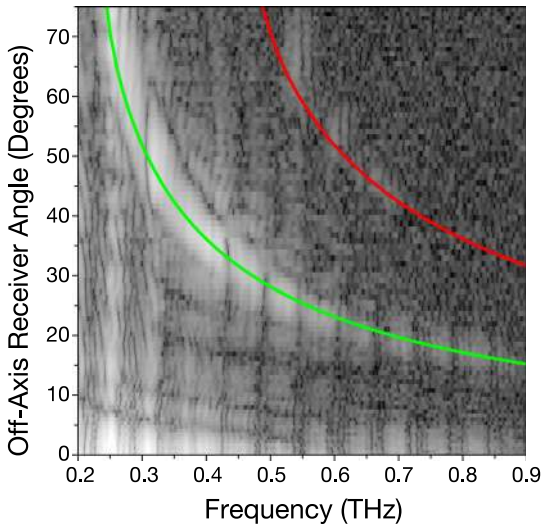

FIG. 5. The spectra of the differential signals diffracted at various receiver angles, when applying an alternating bias at 1 kHz to the device, with gray-scale representing the THz electric field amplitude on a logarithmic scale. The AC bias was applied to alternate columns. The prominent features at small angles from the axis indicate the normally transmitted beam. The arc, dropping from large angles at low frequency to smaller angles at high frequency, represents the angle and frequency dependent broadband first-order diffraction from the device. Also illustrated is the weaker second-order diffraction. The colored curves show the theoretically expected diffraction angle vs. frequency curves for first-order (green) and second-order (red) diffraction.

also be diffracted at angles determined by the grating equation. Consequently, we expect to be able to measure a diffracted signal in a wide range of angles, with different spectral components diffracting in different directions. This is confirmed by the data in Fig. 5, which shows the spectrally resolved measurements as a function of angle. This data set was acquired by applying the AC bias to alternate columns, measuring the differential signal (using the second method), as in Fig. 4(a). This figure clearly shows the signature of THz radiation diffracted over a broad spectral bandwidth, with the diffracted signal continuously shifting to larger angles with increasing wavelength, as expected. A weaker second-order diffraction signature is also observed at larger angles. The theoretically predicted relation between the frequency and the angle of diffraction is shown in the figure for the first two diffraction orders (green and red lines, respectively). This result confirms the broadband nature of the modulation imposed upon the THz field by the metamaterial.

Further, using the first method, with a DC bias on the device, we can estimate the overall diffraction efficiency of the grating. At the design frequency of 0.4 THz, and at the optimal diffraction angle of 36.1°, the power diffraction efficiency is approximately 0.53%. This value obviously has room for improvement, possibly by stacking multiple metamaterial layers or further optimizing the resonance by adjusting the eSRR and epilayer parameters. The insertion loss of the device is 9.4 dB, due in part to the back-surface reflection, as noted above. Further improvement is possible by implementing other strategies of device architecture, for instance, using freestanding thin-film metamaterials exhibiting anomalous refraction.[23]

In conclusion, we have demonstrated a diffractive modulator for THz radiation based on a switchable planar metamaterial. At the metamaterial resonance frequency, this modulator provides a dynamic range in excess of 20 dB, the largest yet reported for an electrically driven THz modulator. The device also exhibits broadband performance, due to the combination of amplitude and phase modulation properties of the metamaterial. Our results indicate that the dynamic range and the diffraction efficiency are not strongly frequency-dependent over a range of at least several hundred GHz, due to the correlated amplitude and phase response of the eSRR array. The freedom to tailor the metamaterial resonances and pixelization offers a powerful strategy for further optimization of the device performance.

This work was performed, in part, at the Center for Integrated Nanotechnologies, an Office of Science User Facility operated for the U.S. Department of Energy (DOE) Office of Science. Part of this work has been supported by the National Science Foundation.

[1]M. Tonouchi, Nat. Photonics **1**, 97 (2007).
[2]R. Kersting, G. Strasser, and K. Unterrainer, Electron. Lett. **36**, 1156 (2000).
[3]T. Kleine-Ostmann, K. Pierz, G. Hein, P. Dawson, M. Marso, and M. Koch, J. Appl. Phys. **105**, 093707 (2009).
[4]C.-F. Hsieh, R.-P. Pan, T.-T. Tang, H.-L. Chen, and C.-L. Pan, Opt. Lett. **31**, 1112 (2006).
[5]B. Sensale-Rodriguez, R. Yan, M. M. Kelly, T. Fang, K. Tahy, W. S. Hwang, D. Jena, L. Liu, and H. G. Xing, Nat. Commun. **3**, 780 (2012).
[6]W. Gao, J. Shu, K. Reichel, D. V. Nickel, X. He, G. Shi, R. Vajtai, P. M. Ajayan, J. Kono, D. M. Mittleman, and Q. Xu, "High-Contrast Terahertz Wave Modulation by Gated Graphene Enhanced by Extraordinary Transmission through Ring Apertures," Nano Lett. (in press).
[7]H.-T. Chen, W. J. Padilla, J. M. O. Zide, A. C. Gossard, A. J. Taylor, and R. D. Averitt, Nature **444**, 597 (2006).
[8]H.-T. Chen, S. Palit, T. Tyler, C. M. Bingham, J. M. O. Zide, J. F. O'Hara, D. R. Smith, A. C. Gossard, R. D. Averitt, W. J. Padilla, N. M. Jokerst, and A. J. Taylor, Appl. Phys. Lett. **93**, 091117 (2008).
[9]H.-T. Chen, W. J. Padilla, M. J. Cich, A. K. Azad, R. D. Averitt, and A. J. Taylor, Nat. Photonics **3**, 148 (2009).
[10]S. H. Lee, M. Choi, T.-T. Kim, S. Lee, M. Liu, X. Yin, H. K. Choi, S. S. Lee, C.-G. Choi, S.-Y. Choi, X. Zhang, and B. Min, Nature Mater. **11**, 936 (2012).
[11]M. Rahm, J.-S. Li, and W. J. Padilla, J. Infrared, Millimeter, Terahertz Waves **34**, 1 (2013).
[12]D. R. Smith, J. B. Pendry, and M. C. K. Wiltshire, Science **305**, 788 (2004).
[13]V. M. Shalaev, Nat. Photonics **1**, 41 (2007).
[14]H.-T. Chen, J. F. O'Hara, A. K. Azad, and A. J. Taylor, Laser Photonics Rev. **5**, 513 (2011).
[15]H.-T. Chen, H. Lu, A. K. Azad, R. D. Averitt, A. C. Gossard, S. A. Trugman, J. F. O'Hara, and A. J. Taylor, Opt. Express **16**, 7641 (2008).
[16]J. Shu, C. Qiu, V. Astley, D. Nickel, D. M. Mittleman, and Q. Xu, Opt. Express **19**, 26666 (2011).
[17]H. Tao, A. C. Strikwerda, K. Fan, W. J. Padilla, X. Zhang, and R. D. Averitt, Phys. Rev. Lett. **103**, 147401 (2009).
[18]M. Seo, J. Kyoung, H. Park, S. Koo, H.-S. Kim, H. Bernien, B. J. Kim, J. H. Choe, Y. H. Ahn, H.-T. Kim, N. Park, Q.-H. Park, K. Ahn, and D.-S. Kim, Nano Lett. **10**, 2064 (2010).
[19]T. Driscoll, H.-T. Kim, B.-G. Chae, B.-J. Kim, Y.-W. Lee, N. M. Jokerst, S. Palit, D. R. Smith, M. Di Ventra, and D. N. Basov, Science **325**, 1518 (2009).
[20]W. L. Chan, H.-T. Chen, A. J. Taylor, I. Brener, M. J. Cich, and D. M. Mittleman, Appl. Phys. Lett. **94**, 213511 (2009).
[21]A. E. Siegman, *Lasers* (University Science Books, 1986)
[22]H.-T. Chen, J. F. O'Hara, A. J. Taylor, R. D. Averitt, C. Highstrete, M. Lee, and W. J. Padilla, Opt. Express **15**, 1084 (2007).
[23]N. K. Grady, J. E. Heyes, D. R. Chowdhury, Y. Zeng, M. T. Reiten, A. K. Azad, A. J. Taylor, D. A. R. Dalvit, and H.-T. Chen, Science **340**, 1304 (2013).